Precipitation of Cerium Oxide nanoparticles by SAS process

Ignacio García-Casas *; Antonio Montes; Diego Valor; Clara Pereyra; Enrique J. Martínez de la Ossa.

Chemical Engineering and Food Technology Department
University of Cadiz. Avda. República Saharaui, s/n, 11510, Puerto Real, Cádiz, SPAIN

*Corresponding author: ignacio.casas@uca.es

Cerium oxide nanoparticles could put a stop to tooth cavities. These nanoparticles could inhibit the formation of the biofilm on teeth, known as plaque, created by bacteria. In this work, nanoparticles of cerium oxide were generated using Supercritical antisolvent (SAS) process followed by a calcination process. The use of supercritical fluids and particularly SAS process to prepare nanoparticles removes the drawbacks of the conventional techniques such as excessive use of solvent, thermal solute degradation, high residual solvent concentration, and mainly difficulty in controlling the particle size and particle size distribution during processing. In the first step, nanoparticles of cerium oxide have been precipitated by SAS process. In this preliminary work, the influence of the pressure on the particle size, particle size distribution, morphology, and specific surface area of these particles have been investigated. Most of the experiments led to successful precipitation of a cluster of particles in the nanometer range. In general, the morphology was greatly improved to spherical nanoparticles. Particle size was higher when the pressure was lower. The specific surface area increases dramatically after the SAS process, from 0.46 m^2/g to a gap between 27 m^2/g and 197 m^2/g.

1. Introduction

Nanoscience and Nanotechnology are currently one of the main focuses of attention of the scientific, industrial and business community due to advances in the synthesis and manipulation of materials at the nanoscale, with multiple applications in the near future. Nanomaterials present characteristics that differentiate them from macro materials, and thus, the same material at nanoscale modifies its electrical, magnetic, optical, and catalytic properties, among others, and these properties are used in fields as diverse as electronics, biomedicine, pharmaceuticals, catalysis, and energy.

In recent years, the study of cerium nanoparticles has expanded beyond their use as a catalyst as Dowding et al. (Dowding et al., 2013) that used nanoparticles of cerium oxide to accelerate the decay of peroxynitrite. Ta et al. (Ta et al., 2013) tuned the shape of ceria nanomaterials for different catalytic applications. The use of cerium dioxide nanoparticles has expanded its use in medical or pharmaceutical fields. Sehar et al. (Sehar et al., 2021) shows the efficiency of these nanoparticles in decreasing photodegradation and bacterial activity. In this way antibacterial activity of these particles of ceria against wound pathogens (Sharma et al., 2020) or Escherichia coli showed by Senthilkumar et al. (Senthilkumar et al., 2019). Cerium nanoparticles have been also used in advances in tissue engineering (Hosseini & Mozafari, 2020) or in biosynthesis and biomedical application (Singh et al., 2020). Even, a recent article links nanoceria as an agent for the management of covid-19 (Allawadhi et al., 2020).

Supercritical CO_2 (scCO_2) has been widely applied to produce nanoparticles of nutraceuticals, pharmaceuticals, metallic, polymers, etc. It has low cost, low toxicity and fairly low critical temperature (31.1 ˚C) and pressure (73.8 bar), which makes it quite adequate for processing thermolabile solutes in environmental agreement (Jung & Perrut, 2001). In addition, the use of scCO_2 processes provides distinct advantages, such as greater product

quality in terms of purity, more homogeneous dimensional characteristics, and its properties can also be continuously tuned by altering the experimental conditions (Cocero et al., 2009).

SAS process has been already used to precipitate metallic nanoparticles (Rueda et al., 2014) using micronized magnesium acetate as precursor for the production of magnesium oxide and magnesium hydrate. Jiang et al. (Jiang et al., 2014) utilized the same process to precipitate a series of manganese–cerium oxide (MnO_x– CeO_2) catalysts used for low temperature selective catalytic reduction (SCR) of NO_x with NH_3. Franco et al. (Franco et al., 2018; Palma et al., 2017) precipitated the same particles, $Ce(acac)_3$ using SAS process. They studied the effect of concentration and flow rate on particle size and granulometric distribution. Its TEM images showed a particle size around 50nm. Finally, these nanoparticles were used as catalyst support for water shift reaction.

In the present work, the direct influence of pressure on the morphology, size and distribution of nanoparticles were studied. At the same time, the greatest significance in the results obtained is reached in the specific surface area of the nanoparticles. The remarkable increase in its specific surface area after using the SAS technique, and the possibility of using supercritical impregnation techniques, make this technique a very useful method to functionalize this kind of nanoparticles.

2. Material and methods

2.1. Materials

Cerium(III) acetylacetonate hydrate ($Ce(C_5H_7O_2)_3 \cdot xH_2O$) and ethanol absolute were supplied by Sigma-Aldrich (Spain). Carbon dioxide (99.8%) was purchased from Abello-Linde S.A. (Barcelona, Spain).

2.2. Supercritical particle formation

Experiments were carried out in a lab-scale high-pressure equipment (SAS200) provided by Thar Technologies (Pittsburgh, PA, USA) (Figure 1). The SAS 200 pilot plant includes two high-pressure pumps to pump the CO_2 (P1) and the solution (P2); a stainless steel precipitator vessel (V1) (0.5 L volume) where the powder is gathered, composed by two main parts, a cylinder body and the frit, all enclosing by an electrical heating jacket (V1-HJ1); an automated high-precision back-pressure regulator (ABPR1) connected to a controller; a jacketed (CS1-HJ1) stainless steel cyclone separator (CS1) (0.5 L volume). SAS was used to precipitate nanoparticles of $Ce(acac)_3$. In this technique, CO_2 was pumped into the vessel and when supercritical conditions were achieved, the cerium solution was pumped into the precipitator vessel by a nozzle. The small drops of solvent were dissolved by the supercritical CO_2, causing supersaturation of the liquid solution and consequent precipitation in the form of a powder that accumulated on the internal wall of the vessel.
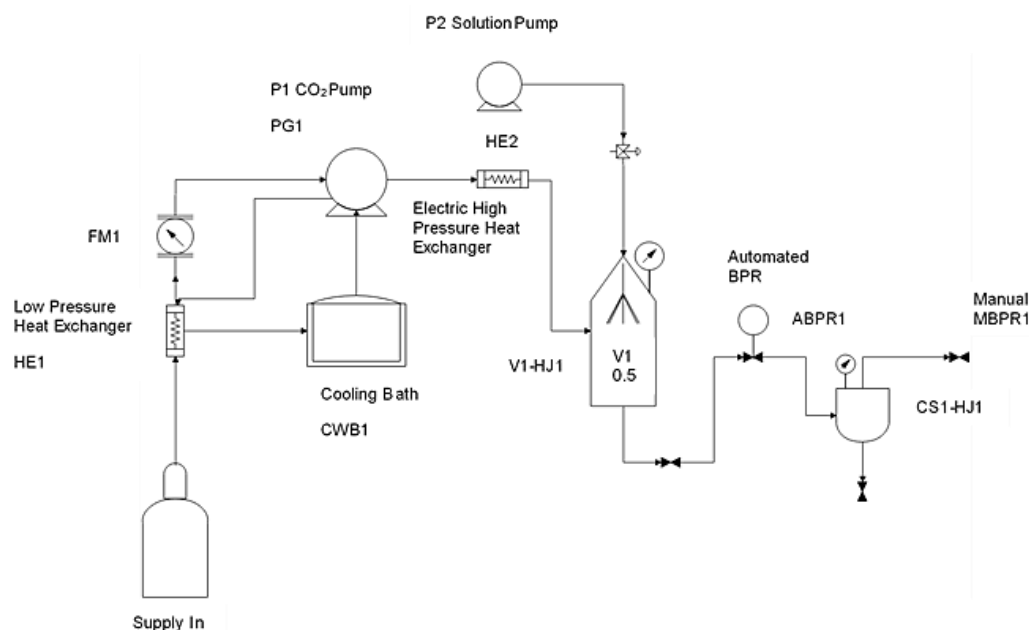
Figure 1. Schematic diagram SAS200 lab-scale plant

In this work, Ce(acac)$_3$ was dissolved in ethanol at concentrations of 3-6 mg/mL. Injection flow rates of 2-6 mL/min for scCO$_2$ were used. The conditions of CO$_2$ flow rate at 20 g/min and a drying time of 30 min were kept constant. These particles were then calcined in a muffle oven at 673 K for 2 h, with a heating ramp of 10 K/min.

2.3. Morphology and particle size

Nanoparticles of Ce(acac)$_3$ were analysed by SEM (FEI Teneo) in order to analyse the morphology and structure of the nanoparticles. The particle size was analysed by a dynamic light scattering (DLS) with Zetasizer Nano Z.

2.4. X-Ray Diffraction

X-ray diffraction (XRD) analysis was performed on a Bruker D8 advance diffractometer to establish the identity and purity of the synthesized samples of the oxide nanoparticles obtained by SAS and calcined process. The diffraction design was measured with CuKα radiation (40Kv, 40mA), 2Ө angle range from 20º to 75º with a step size of 0.02º and 1 s as step time.

2.5. Nitrogen Physisorption

Specific surfaces areas and porosity were measured by ASAP 2420 system. The physical principle of measurement is the adsorption of molecules of a gas in a solid sample. In this study, nitrogen adsorption-desorption isotherms were recorded at 77.35 K. The nanoparticles of Ce(acac)$_3$ and CeO$_2$ powder was pre-treated at 393 K for 3 hours. The specific surface area was determined by the BET method. Microporosity was calculated by t-plot method.

3. Results and discussion

3.1. Study of the precipitated nanoparticles

In this preliminary work, six experiments were carried out to study the effect of the pressure in the formation of Ceria nanoparticles. In a previous work (Yeo et al., 2000) determined that the critical point of the mixture CO$_2$ + ethanol for X_A concentrations of 0.956 is 77.73 bar at 310.58 K, while for an X_A of 0.938, the critical point is 86.35 bar at 318.24 K. To be sure that the experiments would be performed above MCP, the minimum pressure and temperature conditions were fixed at 100 bar and 308 K. The Table 1 shows the experiments and the average size obtained. The nanoparticles show an average size between 133-328 nm. It was observed that in the three pairs of experiments (1-2, 3-4, 5-6), each pair at the same conditions, varying only the pressure, shows that with increasing pressure, the average size of the nanoparticles decreases.

Table 1.Experiments carried out by SAS process. Exp (1-2) 308 K, 3 mg/mL, 6 mL/min; Exp (3-4) 308 K, 6 mg/min, 2 mL/min; (5-6) 323 K, 3 mg/mL, 2 mL/min

Experiments	Pressure (bar)	Particle Size (nm)
1	100	156 ± 46
2	180	133 ± 64
3	100	328 ± 67
4	180	198 ± 72
5	100	281 ± 91
6	180	230 ± 64

The transmission electron microscopy shows in all experiments a cluster of spherical nanoparticles. In Figure 2A and 2B, it can be observed the nanoparticles precipitated in experiment 2 at 180 bar, experiment 1, at 100 bar and the raw Ce(acac)$_3$ before SAS process (Figure 2C), that shows nanoparticles but also sticks particles of around 1 μm.
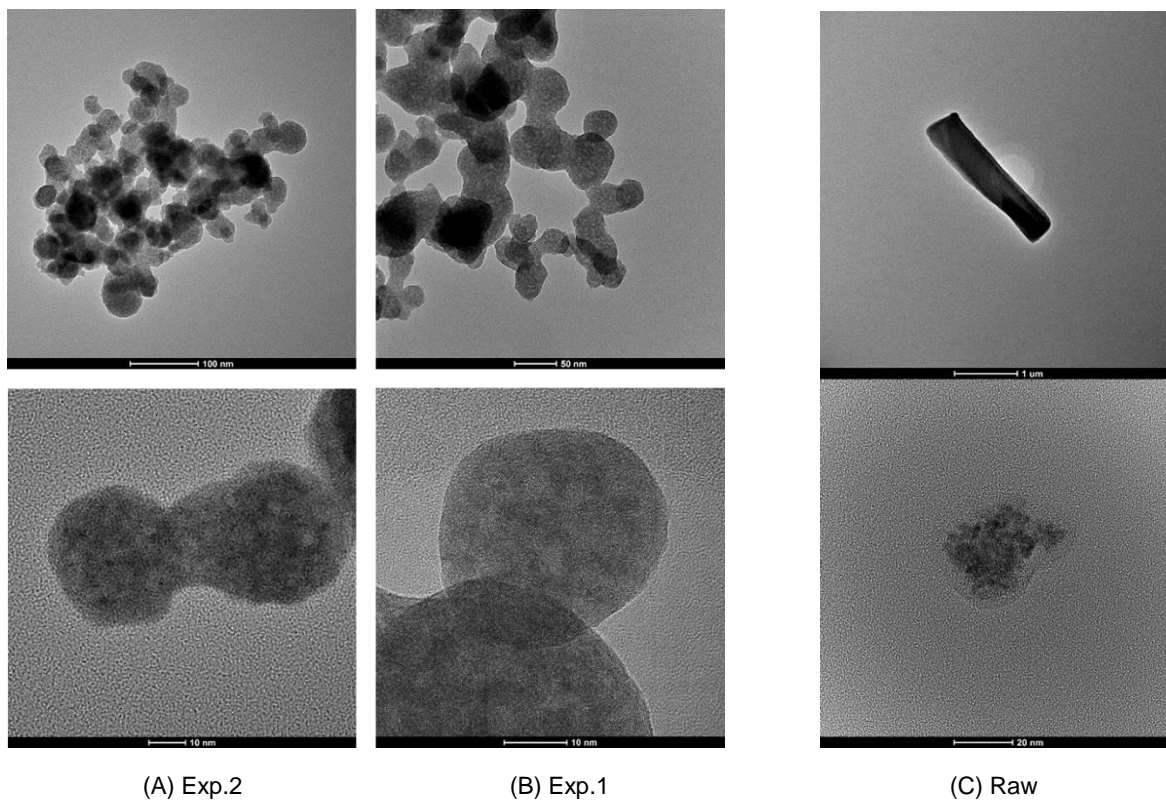
(A) Exp.2   (B) Exp.1   (C) Raw

Figure 2. TEM images of Experiments 1, 2 and Raw Ce(acac)$_3$

3.2. Samples Characterization

XRD analysis was presented in Figure 3. The diffractogram shows four peaks that are labeled and can be identified and indexed as the face-centered cubic phase (Goharshadi et al., 2011). The clear strong and sharp diffraction peaks denote the good crystallization of the sample. No extra peaks were detected in the XRD, indicating a good purity of the prepared ceria nanoparticles.
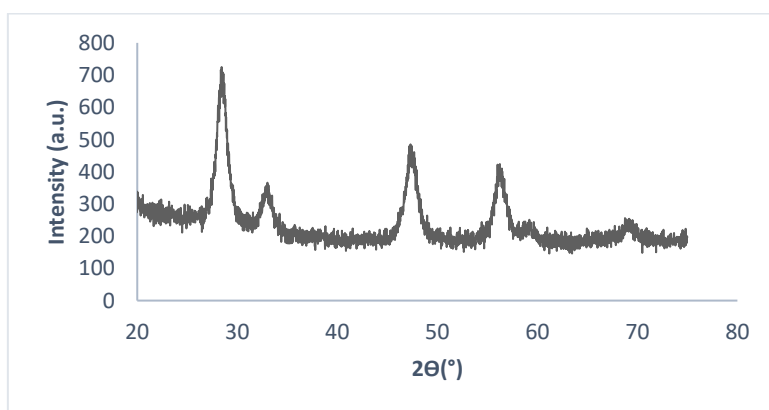

Figure 3. XRD analysis of experiment 4 calcined

In the physisorption study (Table 2), it can be observed that for all experiments the specific surface area increases very significantly after precipitating the cerium compound with the SAS technique. The commercial Ce(acac)$_3$ has a specific surface area of 0.43 m$_2$/g, while the nanoparticles obtained range from 27 m$_2$/g in experiment 6 to 192 m$_2$/g in experiment 4. In this case, it seems that the operating pressure, always under supercritical conditions, does not clearly affect the specific surface area of the nanoparticles.

On the other hand, it was studied the specific surface of the nanoparticles of cerium dioxide obtained in experiments 3 and 4 after calcination. Both experiments show a reduction of the specific surface area after calcination. Experiment 3 reduces its specific surface area from 66 m2/g to 25 m2/g, while experiment 4 reduces it from 192 m2/g to 43m2/g. As can be expected, the average pore size in the supercritical Ce(acac)3 tests decreases, which favors the increase of the specific surface area. Similarly, the average pore size increases in experiments 3 and 4, once oxidized, from 10.04 nm to 23.67 nm and from 5.92 nm to 18.51 nm respectively, which leads to a reduction of their specific surface area.

Table 2. Physisorption results for SAS experiments of Ce(acac)$_3$ and CeO$_2$

Experiments	Pressure (bar)	Specific Surface Area (m$_2$/g)	Average Pore Size (nm)
Raw		0.43	26.61
1	100	141	11.31
2	180	166	12.20
3	100	66	10.04
4	180	192	5.92
5	100	113	13.21
6	180	27	13.17
3 Calcined		25	23.67
4 Calcined		43	18.51

4. Conclusions

In this preliminary work the formation of cerium dioxide particles using the SAS technique and the influence of pressure on the average size of the obtained nanoparticles was achieved with a wide range of conditions, always under supercritical conditions. These nanoparticles showed a decrease in the average size by increasing the pressure. The exponential increase of the specific surface area for both Ce(acac)$_3$ and CeO$_2$ nanoparticles, with respect to commercial Ce(acac)$_3$, opens the possibility of functionalizing these nanoparticles by impregnating them due to the significant increase of the specific surface area.

References

Allawadhi, P., Khurana, A., Allwadhi, S., Joshi, K., Packirisamy, G., & Bharani, K. K., 2020. Nanoceria as a possible agent for the management of COVID-19. *Nano Today*, *35*.

Cocero, M. J. M. J., Martín, Á., Mattea, F., Varona, S., 2009. *Encapsulation and co-precipitation processes with supercritical fluids: Fundamentals and applications*. *47*(3), 546–555.

Dowding, J. M., Seal, S., & Self, W. T., 2013. Cerium oxide nanoparticles accelerate the decay of peroxynitrite (ONOO$^-$). *Drug Delivery and Translational Research*, *3*(4), 375–379.

Franco, P., Martino, M., Palma, V., Scarpellini, A., & De Marco, I., 2018. Pt on SAS-CeO$_2$ nanopowder as catalyst for the CO-WGS reaction. *International Journal of Hydrogen Energy*, *43*(43), 19965–19975.

Goharshadi, E. K., Samiee, S., & Nancarrow, P., 2011. Fabrication of cerium oxide nanoparticles: Characterization and optical properties. *Journal of Colloid and Interface Science*, *356*(2), 473–480.

Hosseini, M., & Mozafari, M., 2020. Cerium oxide nanoparticles: Recent advances in tissue engineerings. *Materials*, *13*(14).

Jiang, H., Zhao, J., Jiang, D., & Zhang, M., 2014. Hollow MnO$_x$-CeO$_2$ nanospheres prepared by a green route: A novel low-temperature NH$_3$-SCR catalyst. *Catalysis Letters*, *144*(2), 325–332.

Jung, J., & Perrut, M., 2001. Particle design using supercritical fluids: Literature and patent survey. *The*

Journal of Supercritical Fluids, *20*(3), 179–219.

Palma, V., Pietrosanto, A., Martino, M., Reverchon, E., & De Marco, I., 2017. Supercritical antisolvent process to produce cerium oxide nanoparticles as a support for high-activity platinum catalysts. *Chemical Engineering Transactions*, *57*, 967–972.

Rueda, M., Sanz-Moral, L. M., & Martín, Á., 2014. Micronization of magnesium acetate by the supercritical antisolvent process as a precursor for the production of magnesium oxide and magnesium hydride. *Crystal Growth and Design*, *14*(9), 4768–4776.

Sehar, S., Naz, I., Rehman, A., Sun, W., Alhewairini, S. S., Zahid, M. N., & Younis, A., 2021. Shape-controlled synthesis of cerium oxide nanoparticles for efficient dye photodegradation and antibacterial activities. *Applied Organometallic Chemistry*, *35*(1).

Senthilkumar, R. P., Bhuvaneshwari, V., Malayaman, V., Chitra, G., Ranjithkumar, R., Dinesh, K. P. B., & Chandarshekar, B., 2019. Biogenic method of cerium oxide nanoparticles synthesis using wireweed (Sida acuta Burm.f.) and its antibacterial activity against Escherichia coli. *Materials Research Express*, *6*(10).

Sharma, G., Prema, D., Venkataprasanna, K. S., Prakash, J., Sahabuddin, S., & Devanand Venkatasubbu, G., 2020. Photo induced antibacterial activity of CeO_2/GO against wound pathogens. *Arabian Journal of Chemistry*, *13*(11), 7680–7694.

Singh, K. R. B., Nayak, V., Sarkar, T., & Singh, R. P., 2020. Cerium oxide nanoparticles: Properties, biosynthesis and biomedical application. *RSC Advances*, *10*(45), 27194–27214.

Ta, N., Liu, J., & Shen, W., 2013. Tuning the shape of ceria nanomaterials for catalytic applications. *Cuihua Xuebao/Chinese Journal of Catalysis*, *34*(5), 838–850.

Yeo, S. Do, Park, S. J., Kim, J. W., & Kim, J. C., 2000. Critical properties of carbon dioxide+methanol, +ethanol, +1-propanol, and +1-butanol. *Journal of Chemical and Engineering Data*, *45*(5), 932–935.